Available online at www.sciencedirect.com
SCIENCE DIRECT®
Journal of Computational Physics 201 (2004) 13–33
JOURNAL OF COMPUTATIONAL PHYSICS
www.elsevier.com/locate/jcp

Newton–Krylov continuation of periodic orbits for Navier–Stokes flows

J. Sánchez [a,*], M. Net [a], B. García-Archilla [b], C. Simó [c]

[a] *Departament de Física Aplicada, Universitat Politècnica de Catalunya, Jordi Girona Salgado 1–3, Campus Nord UPC, Mòdul B4–B5, 08034 Barcelona, Spain*

[b] *Departamento de Matemática Aplicada II, Universidad de Sevilla, Escuela Superior de Ingenieros, Camino de los Descubrimientos, s/n, 41092 Sevilla, Spain*

[c] *Departament de Matemàtica Aplicada i Anàlisi, Universitat de Barcelona, Gran Via de les Corts Catalanes, 585, 08071 Barcelona, Spain*

Received 17 December 2003; received in revised form 26 April 2004; accepted 29 April 2004
Available online 11 June 2004

Abstract

Efficient numerical algorithms for the continuation of periodic orbits of high-dimensional dissipative dynamical systems, and for analyzing their stability are presented. They are based on shooting, Newton–Krylov and Arnoldi methods. A thermal convection fluid dynamics problem, which has a rich bifurcation diagram due to symmetries, has been used as test. After a pseudo-spectral discretization of the equations a system of dimension $O(10^4)$ has been obtained. The efficiency of the algorithms, which allows the unfolding of a complex diagram of periodic orbits, makes the methods suitable for the study of large nonlinear dissipative partial differential equations.

Keywords: Continuation methods; Periodic orbits; Poincaré maps; Variational equations; Krylov methods; Arnoldi decomposition; Subspace iteration

1. Introduction

The study of any dynamical system involves the computation of its invariant manifolds (fixed points, periodic orbits, homo and heteroclinic orbits, invariant tori, etc.), and the study of their persistence and changes of stability when the parameters on which the problem depends are varied. Unstable manifolds must also be calculated because they may drive the dynamics of the system or give rise to stable solutions as will be seen in the examples shown here. Some of these tasks are now almost routinely performed for low-dimensional problems. Many researchers in dynamical systems have benefited from the availability of

* Corresponding author. Tel.: +34-93-4017981; fax: +34-93-4016090.
E-mail address: sanchez@fa.upc.es (J. Sánchez).

0021-9991/$ - see front matter
doi:10.1016/j.jcp.2004.04.018

continuation and bifurcation packages such as AUTO [7], CONTENT [16], DSTOOL [9], etc. Due to the small size of the systems they are designed for, they implement direct solvers for the linear problems involved in the computations (linear algebraic systems and eigenvalue problems). The extension to high-dimensional problems is not straightforward, the main obstacle being the computational cost of the linear algebra. The development of modern linear algebra techniques, many of them based on Krylov or Arnoldi methods [28,30], allow the study of large systems such as those in computational fluid dynamics. This is the case of some works that have appeared in the last years, most of them dealing with the computation of steady states in fluid flows or reaction-diffusion problems. Inexact Newton–Krylov methods are used to find the fixed points and the Arnoldi method to study their stability [2,8,21,23]. The main difficulty is always to achieve a fast convergence of the linear solvers (GMRES [31] in many cases). Preconditioning is then mandatory and its nature depends on how space variables are discretized. For spectral discretizations in incompressible fluid problems, [8] suggest the use of the Stokes operator as preconditioner. This is the method employed, for example, in [23]. The use of preconditioners based on finite differences or elements within a spectral method is also a possibility. This approach is involved because the equations defining the system must be discretized in two distinct ways. In the case of finite differences or finite elements, incomplete LU decompositions provide reliable preconditioners [25,29,32].

Continuations of periodic orbits in large-scale dissipative systems have also been performed in a few problems ([22,40] for instance) of moderate dimension, which, in some cases, can still be integrated in time with library routines for stiff systems of ordinary differential equations. These studies use the Newton–Picard algorithm described in [22], which is based on a modification of the recursive projection method (RPM) [33]. More recently [38,39,41], a limited memory Broyden method has also been employed to compute periodic orbits for high-dimensional systems. In this work, we present an alternative to those methods. We apply Newton–Krylov techniques to obtain the fixed points of a Poincaré map. Because of the dissipative nature of the problems the methods are addressed to, their Floquet multipliers are clustered around the origin. Therefore, there are two main differences with the computation of fixed points. There is no need for preconditioning the iterative solver for the linear systems at each Newton's iteration, and there is no need to make shift-invert or Cayley transformations [24] to find the spectra. In this sense it is easier to compute periodic orbits than steady solutions as only a time stepping code is needed. The evaluation of the functions involved is, obviously, much more expensive because it implies the time integration of the equations over a period of the orbit.

We apply these algorithms to compute a complex bifurcation diagram of periodic orbits and to study their stability in a non-trivial fluid dynamics problem of dimension $O(10^4)$. Specifically, we consider thermal convection in a bidimensional cylindrical annular domain driven by a difference of temperature externally imposed on its boundaries.

The layout of the paper is as follows. In Section 2 we describe the continuation method used to find the periodic orbits and to study their stability, including the arguments that justify the good convergence properties observed in the applications. In Section 3 we introduce the problem to which the method has been applied, the spatial discretization and the time integration algorithm employed. The results obtained are presented in Section 4. Discussion on the efficiency of the numerical method is done in Section 5. Finally, the paper closes in Section 6 with a summary of the results and a brief description of some possible extensions.

2. Continuation method for periodic orbits

Consider a finite dimensional autonomous dynamical system with governing equations

$$B\dot{x} = f(x,\lambda) = L(\lambda)x + Q(x,x) + F, \tag{1}$$

with $(x,\lambda)\in\mathscr{U}\subset\mathbb{R}^n\times\mathbb{R}$, and where $L(\lambda)$ and Q are linear and quadratic operators respectively with $Q(0,0)=0$ and $D_xQ(0,0)=0$, F is a constant forcing term, and B a constant linear operator. We also suppose that the dependence of the problem on λ, which may be any of the governing parameters of the problem, is of the form

$$L(\lambda)=L_1+\lambda L_2, \tag{2}$$

where L_1 and L_2 are linear operators independent of λ.

Although the method here described is of general applicability, the calculation of the derivatives of the right hand side of (1), needed to integrate its first variational equations, are trivial in this particular form. Many reaction-diffusion, and fluid mechanics problems can be formulated in this way. The operators $L(\lambda)$ and Q could be the discretized versions of the continuous operators of a system of partial differential equations (PDE). B might be singular if, for instance, an incompressible velocity–pressure formulation of the Navier–Stokes equations is employed giving rise to a differential–algebraic system, or invertible in the case of streamfunction or scalar potential formulations. Even these latter constitute differential–algebraic systems depending on how the boundary conditions are implemented.

Periodic orbits of (1) are obtained as fixed points of a Poincaré map on a section Σ, which for simplicity is taken as a hyperplane. If x_σ is a point close to an initial periodic orbit, and ω_σ is such that the hyperplane Σ given by

$$g(x)=\omega_\sigma^{\mathrm{T}}(x-x_\sigma)=0, \tag{3}$$

is transverse to the flow of (1), the Poincaré map, $P:\mathscr{V}\subset\Sigma\to\Sigma$, is defined as

$$P(x,\lambda)=\varphi(t(x),x,\lambda), \tag{4}$$

where $x\in\mathscr{V}$, $\varphi(t,x,\lambda)$ is the solution of (1) with initial condition $x=\varphi(0,x,\lambda)$, $t(x)$ is the minimal time verifying $t(x)>0$ and $z=\varphi(t(x),x,\lambda)\in\Sigma$, with $\omega_\sigma^{\mathrm{T}}\partial_t\varphi(0,x,\lambda)$ and $\omega_\sigma^{\mathrm{T}}\partial_t\varphi(t(x),z,\lambda)$ having the same sign. The particular form of computing $t(x)$ and $\varphi(t(x),x,\lambda)$ depends on the time integration method used. The periodic orbits are then given by

$$x-P(x,\lambda)=0,\quad x\in\Sigma. \tag{5}$$

To solve these equations the hyperplane Σ must be parametrized. Let $\omega_{\sigma k}$ be a non-vanishing component of ω_σ. It can be selected, for instance, verifying $|\omega_{\sigma k}|=\max_{i=1,\dots,n}|\omega_{\sigma i}|$. Let R_k be the projection of Σ onto $\mathbb{R}^{n-1}$, $R_k:\Sigma\to\mathbb{R}^{n-1}$, defined by

$$R_k(x_1,\dots,x_{k-1},x_k,x_{k+1},\dots,x_n)=(x_1,\dots,x_{k-1},x_{k+1},\dots,x_n),$$

$\bar{x}=R_k(x)$, and E_k the map, $E_k:\mathbb{R}^{n-1}\to\Sigma$, defined by

$$E_k(x_1,\dots,x_{k-1},x_{k+1},\dots,x_n)=\left(x_1,\dots,x_{k-1},x_{\sigma k}-\frac{\bar{\omega}_\sigma^{\mathrm{T}}(\bar{x}-\bar{x}_\sigma)}{\omega_{\sigma k}},x_{k+1},\dots,x_n\right),$$

with $\bar{\omega}_\sigma=R_k(\omega_\sigma)$ and $\bar{x}_\sigma=R_k(x_\sigma)$. These maps are diffeomorphisms and verify $R_k\circ E_k=I_{\mathbb{R}^{n-1}}$, $E_k\circ R_k=I_\Sigma$, $DR_k(x)=R_k$, and

$$DE_k(\bar{x})(u_1,\dots,u_{k-1},u_{k+1},\dots,u_n)=\left(u_1,\dots,u_{k-1},-\frac{\bar{\omega}_\sigma^{\mathrm{T}}\bar{u}}{\omega_{\sigma k}},u_{k+1},\dots,u_n\right)$$

if $\bar{u}=(u_1,\dots,u_{k-1},u_{k+1},\dots,u_n)$.

If we now define $\bar{P}(\bar{x},\lambda) = R_k(P(E_k(\bar{x}),\lambda))$ then $D_{\bar{x}}\bar{P}(\bar{x},\lambda) = R_k(D_{\bar{x}}P(x,\lambda)DE_k(\bar{x}))$ with $x = E_k(\bar{x})$, and the fixed points of $\bar{P}$, verifying

$$\bar{x} - \bar{P}(\bar{x},\lambda) = 0, \quad \bar{x} \in \mathbb{R}^{n-1}, \tag{6}$$

are in one-to-one correspondence with those of P by the map $x = E_k(\bar{x})$.

Predictor-corrector parameter and pseudo-arclength continuation methods [14] are used to study the dependence of the solutions of (6) on the parameter λ. Second degree polynomial extrapolation with respect to the arclength, s, is used as predictor and Newton's method as corrector. They admit a unified formulation by adding the equation

$$n(\bar{x},\lambda) \equiv \theta\omega_{\bar{x}}^{\mathrm{T}}(\bar{x} - \bar{x}_0) + (1-\theta)\omega_\lambda(\lambda - \lambda_0) = 0, \tag{7}$$

$(\bar{x}_0,\lambda_0)$ being the predicted point along the curve of solutions. In the case of parameter continuation $\theta = 0, \omega_\lambda \neq 0$, and λ_0 is the value of the parameter for the next solution. In the case of pseudo-arclength continuation, $(\omega_{\bar{x}},\omega_\lambda)$ is an approximation to the tangent to the curve of solutions $(\bar{x}(s),\lambda(s))$, which can also be approximated by extrapolation, and $0 \leqslant \theta \leqslant 1$ is a parameter that controls the relative weight of $\bar{x}$ and λ in Eq. (7). A widely-used technique is $(\bar{x}_0,\lambda_0) = (\bar{x}_1,\lambda_1) + \Delta s(\omega_{\bar{x}},\omega_\lambda)$, where Δs is the desired increment in the arclength, and $(\bar{x}_1,\lambda_1)$ the last point found. In this case (7) with $\theta = 1/2$ is equivalent to the original formulation of pseudo-arclength, $\omega_{\bar{x}}^{\mathrm{T}}(\bar{x} - \bar{x}_1) + \omega_\lambda(\lambda - \lambda_1) = \Delta s$.

The system that determines a unique solution is then

$$\bar{x} - \bar{P}(\bar{x},\lambda) = 0, \quad n(\bar{x},\lambda) = 0, \qquad \bar{x} \in \mathbb{R}^{n-1}, \tag{8}$$

and the linear system to be solved at each Newton's iteration, $(\bar{x}^{i+1},\lambda^{i+1}) = (\bar{x}^i,\lambda^i) + (\Delta\bar{x}^i,\Delta\lambda^i)$, is

$$\begin{pmatrix} I - D_{\bar{x}}\bar{P}(\bar{x}^i,\lambda^i) & -D_\lambda\bar{P}(\bar{x}^i,\lambda^i) \\ \theta\omega_{\bar{x}}^{\mathrm{T}} & (1-\theta)\omega_\lambda \end{pmatrix} \begin{pmatrix} \Delta\bar{x}^i \\ \Delta\lambda^i \end{pmatrix} = \begin{pmatrix} -\bar{x}^i + \bar{P}(\bar{x}^i,\lambda^i) \\ -n(\bar{x}^i,\lambda^i) \end{pmatrix}. \tag{9}$$

In the case of parameter continuation $\Delta\lambda^i = 0$ and there is no need of $D_\lambda\bar{P}$ in (9).

The linear system (9) is solved iteratively by matrix-free methods that only require the computation of matrix–vector products. Therefore a procedure to compute products of the form $D_xP(x,\lambda)\Delta x^i$ or $D_xP(x,\lambda)\Delta x^i + D_\lambda P(x,\lambda)\Delta\lambda^i$ must be available. For systems of the form (1), they can be obtained, with minor modifications of the time stepping codes employed to integrate them, from a first variational equation. For the system

$$B\dot{x} = f(x,\lambda) = (L_1 + \lambda L_2)x + Q(x,x) + F, \tag{10}$$

$$\dot{\lambda} = 0, \tag{11}$$

with initial condition (x^i,λ^i), the first variational equation is

$$B\dot{y} = D_x f(x,\lambda)y + D_\lambda f(x,\lambda)\mu = (L_1 + \lambda L_2)y + \mu L_2 x + Q(x,y) + Q(y,x), \tag{12}$$

$$\dot{\mu} = 0, \tag{13}$$

with initial condition $(\Delta x^i,\Delta\lambda^i)$. The term $D_\lambda f(x,\lambda)\mu$ must be included in (12) only if pseudo-arclength continuation is used.

If Δx is tangent to $\Sigma, \omega_\sigma^{\mathrm{T}}\Delta x = 0$, then, from the application of the implicit function theorem to the identity $g(\varphi(t(x),x,\lambda)) = 0$ and the definition of $P(x,\lambda)$, we obtain

$$D_xP(x,\lambda)\Delta x + D_\lambda P(x,\lambda)\Delta\lambda = u - \frac{\omega_\sigma^{\mathrm{T}}u}{\omega_\sigma^{\mathrm{T}}z}z, \tag{14}$$

where $u = D_x\varphi(t(x),x,\lambda)\Delta x + D_\lambda\varphi(t(x),x,\lambda)\Delta\lambda$ can be obtained as $u = \hat{\varphi}(t(x),x,\lambda)$, with $\hat{\varphi}(t,x,\lambda)$ solution of (12) with initial condition $y(0) = \Delta x, \mu = \Delta\lambda$. Here z denotes the tangent to $\varphi(t,x,\lambda)$ at $P(x,\lambda)$. It can be obtained from the linear equation $Bz = f(P(x,\lambda),\lambda)$ if B is invertible or, in any case, by interpolation if a multistep time integration method is used. From (14) it is clear that $\omega_\sigma^{\mathrm{T}}(D_xP(x,\lambda)\Delta x + D_\lambda P(x,\lambda)\Delta\lambda) = 0$. See [34] for more details about the computation of the differentials of Poincaré maps and for the case of an arbitrary hypersurface g.

Each evaluation of $D_xP(x,\lambda)\Delta x^i + D_\lambda P(x,\lambda)\Delta\lambda^i$ requires the integration of the $2n$-dimensional system of equations (10) and (12). Because matrix-free methods are employed, only this system must be integrated in time instead of one of dimension n^2+n when the whole first variationals are employed to solve (9) with direct methods. The value of $D_xP(x,\lambda)\Delta x^i + D_\lambda P(x,\lambda)\Delta\lambda^i$ could be computed by finite differences, but the cost is the same because two integrations of (10) are needed. Furthermore the variational estimate of the differential is more accurate than the one obtained by numerical differencing. This implies that if finite differences are employed, the convergence of Newton's method may worsen.

We use GMRES [31] (generalized minimum residual method) to solve all the linear systems. GMRES is an iterative projection method. Given an initial guess y_0 to the solution of the linear system of equations $Ay = b$, this class of methods generate a sequence of approximations y_m which satisfies two conditions

$$y_m \in y_0 + \mathscr{K}_m \quad \text{and} \quad b - Ay_m \perp \mathscr{L}_m, \tag{15}$$

that determine each particular projection method. $\mathscr{K}_m$ and $\mathscr{L}_m$ are two m-dimensional linear subspaces. With these two conditions, y_m minimizes the Euclidean norm of the residual, $b - Ay_m$, over all the vectors in $y_0 + \mathscr{K}_m$. In the particular case of GMRES, $\mathscr{L}_m = A\mathscr{K}_m$ and $\mathscr{K}_m$ is the Krylov subspace $\mathscr{K}_m = \{r_0, Ar_0, A^2r_0, \ldots, A^{m-1}r_0\}$, where $r_0 = b - Ay_0$ (see [28] for implementation details). To prevent the dimension of the subspaces from growing, thus making the method impractical, it is limited to a maximum M. If GMRES does not converge to the desired accuracy in M iterations, the method is restarted using the latest approximation found as initial guess y_0 giving rise to the restarted generalized minimum residual method GMRES(M).

The method described above will only be efficient if the convergence of GMRES is fast enough. The following result (see [30]) can be used to show that, with the particular form of the spectrum of $D_xP(x,\lambda)$ for a dissipative system, the number of iterations needed is much less than the dimension of the system.

Proposition 1. *Suppose that a matrix A is diagonalized as $A = V\Lambda V^{-1}$, where $\Lambda = \mathrm{diag}\{\lambda_1,\ldots,\lambda_n\}$ is the diagonal matrix of eigenvalues, P_m is the set of polynomials of degree at most m, and $\kappa_2(V) = ||V^{-1}||_2||V||_2$ is the norm-2 condition number of V. Then at the m-th step of GMRES*

$$\frac{||b - Ay_m||_2}{||b - Ay_0||_2} \leqslant \kappa_2(V) \inf_{\substack{p\in P_m \\ p(0)=1}} \sup_{i=1,\ldots,n} |p(\lambda_i)|. \tag{16}$$

This result implies that, if there are polynomials of low degree m, which are small enough on the spectrum of A, i.e., $\kappa_2(V)\sup_{i=1,\ldots,n}|p(\lambda_i)| < \varepsilon$, then the residual is reduced at least by a factor ε after a low number of iterations m.

Consider now the linear systems of the form

$$(I - D_xP(x,\lambda))\Delta x = -x + P(x,\lambda), \tag{17}$$

solved in parameter continuation and where, from now on, we drop the over-bars. We can suppose, without loss of generality, that the eigenvalues, μ_i, of $D_xP(x,\lambda)$ have been ordered by non-increasing modulus, so that $|\mu_1| = \max_{i=1,\ldots,n}|\mu_i|$. The eigenvalues of $I - D_xP(x,\lambda)$ are $1 - \mu_i$. They are clustered around $z = 1$ and

are different from zero if the system (1) is derived from the discretization of a dissipative system of PDE's and x is near a regular solution of (5). Therefore, the next proposition, which follows from the principle of the maximum modulus, provides an upper bound for the right hand side of (16).

Proposition 2. *Let* $\mu_1, \ldots, \mu_k$ *be the eigenvalues of* $D_x P(x,\lambda)$ *verifying* $|\mu_i| > \delta$ *with a fixed* $\delta < 1, D = \max_{i=1,\ldots,n} |\mu_i|$ *and* $d = \min_{i=1,\ldots,k} |1-\mu_i|$. *Then the polynomial* $q(z) = (-1)^{k+p}(z-1)^p \prod_{i=1,\ldots,k}(z-1+\mu_i)/(1-\mu_i)$ *verifies* $q(0) = 1$ *and* $\sup_{i=1,\ldots,n} |q(1-\mu_i)| < \delta^p S$, *with* $S = \sup_{|z-1|=\delta} \prod_{i=1,\ldots,k} |z-1+\mu_i|/|1-\mu_i|$. *Moreover,* $S < (\delta + D)^k/d^k$.

By using (16) it follows that $||b - Ay_m||_2/||b - Ay_0||_2 < \varepsilon$ if δ and p chosen so that $\delta^p S < \varepsilon/\kappa_2(V)$, i.e.,

$$m = k + p > k + \log\left(\frac{\kappa_2(V) S}{\varepsilon}\right) / \log(1/\delta). \tag{18}$$

Therefore, if the number of GMRES iterations is larger than m, the residual is reduced, at least, by a factor ε. A rough estimation of m can be obtained by using that $S < (\delta + D)^k/d^k$. The value of D indicates how unstable the orbit is, and d how near singular $I - D_x P(x,\lambda)$ is. Suppose we are looking for not very unstable orbits, so that $D < 10$, and x is not very near a bifurcation, $d > 10^{-2}$ for instance, that we want to reduce the residual by $\varepsilon = 10^{-6}$ and that V is far from normal, as could be expected for large scale dissipative nonlinear PDE, $\kappa_2(V) = 10^{20}$ for instance. Let us take $\delta = 0.1$ and suppose that then $k \approx 40$ (as in some of the spectra we have computed). Therefore we could expect to need, approximately, $m = 200$ iterations to have $||b - Ay_m||_2/||b - Ay_0||_2 < \varepsilon$. This a low value for m for a high-dimensional system. If the spectrum in Fig. 10, in which $k = 40$ eigenvalues have modulus greater that $\delta = 0.15$, is used to estimate S, we find that $S < 4580$ and $m = 88$. In practice we have found that these are conservative lower bounds for m, and fewer iterations are needed to solve the linear systems. As $\kappa_2(V)$ and the distribution of the eigenvalues are not known, a priori, some experiments must be performed to determine good values for the maximal dimension M of K_m. An example will be given later.

The above argument only applies to parameter continuation. With pseudo-arclength continuation the spectrum of the matrix in (9) instead of $I - D_x P(x,\lambda)$ must be considered. We have calculated its dominant eigenvalues for the example in Section 3 at several points of the bifurcation diagram. We have always observed very small perturbations of those of $I - D_x P(x,\lambda)$, except for the appearance of a single new eigenvalue that does not affect the reasoning. The consequence is that we have not observed slower convergences in the case of pseudo-arclength continuation. It is also possible to use compactness arguments on the continuous operators involved to show that both $I - D_x P(x,\lambda)$ and the matrix in (9) have spectra of the kind described above.

Inexact Newton's methods, like those we use, are known to converge if the residual of the linear system to be solved at each Newton's iteration is kept sufficiently small [6]. They can retain quadratic convergence with a suitable selection of the tolerance for the residual. This has been the case in all our computations except, of course, in the neighborhood of bifurcation points. No particular difficulty has been found near turning points.

Summarizing, we can expect to have convergence of the Newton–Krylov method when it is applied to find zeros of $x - P(x)$, with P any map with its multipliers at the fixed point clustered around the origin. In Section 6 we show how to use this fact to compute also steady solutions of (1).

Once the periodic orbits have been obtained, we study their stability by computing their dominant Floquet multipliers by subspace iteration, or by the implicitly restarted Arnoldi iteration [19], using the ARPACK library [20] (see also [1] or [10] for similar computations of Floquet multipliers in another hydrodynamic problem). This also requires the integration of the $2n$-dimensional system (10) and (12). This differs from the method described in [22]. The use of Newton–Picard provides simultaneously the solution

and its stability. With the algorithm we describe, the branches of solutions can be calculated in a first stage, and later use a bisection method along the branch to detect possible bifurcations, if it is needed. This implies studying the stability of only a few solutions in a separate process.

3. The test problem: thermal convection in an annulus

To test the method, the two-dimensional nonlinear thermal convection of a Boussinesq fluid in an annulus, with constant inward radial gravity and heated from the inside, is considered. Its physical interest arises from the study of large-scale motions generated by radial temperature gradients in geophysical and astrophysical processes (see [27,26] for details). The nonlinear dynamics of the two-dimensional vortices also provides a simple fluid dynamical system highly attractive from the point of view of bifurcation theory, because it is large enough to provide a rich spatio-temporal dynamics.

The two-dimensional domain has inner and outer radii R_i and R_o. The three non-dimensional parameters of the problem are the radius ratio, $\eta = R_\mathrm{i}/R_\mathrm{o}$, the Prandtl number, $\sigma = \nu/\kappa$, and the Rayleigh number, $Ra = \alpha\Delta T g d^3/\kappa\nu$, with ν, α and κ the kinematic viscosity, the thermal expansion coefficient, and the thermal diffusivity of the fluid respectively, g a constant radial gravity, ΔT the temperature difference between both boundaries, and d the radii difference. Almost all the results shown in this section correspond to $\eta = 0.3, \sigma = 0.025$, and Ra is taken as the continuation parameter. The values of ΔT, d and d^2/κ are taken as temperature, length and time units, respectively. With this scaling the inner and outer radii are $r_\mathrm{i} = \eta/(1-\eta)$ and $r_\mathrm{o} = 1/(1-\eta)$. From now on, $\mathbf{u}$ and T will be respectively the non-dimensional velocity and temperature fields. The conduction steady state $\mathbf{u}_\mathrm{c} = 0$, $T_\mathrm{c}(r) = T_\mathrm{i} + \ln(r/r_\mathrm{i})/\ln\eta$ is a solution for any value of Ra.

The velocity field $\mathbf{u}$ is written in terms of a streamfunction, Ψ, as $\mathbf{u} = \nabla \times (\Psi \hat{\mathbf{e}}_\mathbf{z})$, where $\hat{\mathbf{e}}_z$ the unit upward vertical vector. Let us define the azimuthal average operator

$$P_\theta g(t,r,\theta) = (2\pi)^{-1} \int_0^{2\pi} g(t,r,\theta)\mathrm{d}\theta.$$

By separating the mean flow $f(t,r) = P_\theta u_\theta(t,r,\theta)$ from Ψ, the preceding expression of $\mathbf{u}$ can be written as $\mathbf{u} = f\hat{\mathbf{e}}_\theta + \nabla \times (\psi \hat{\mathbf{e}}_z)$, with $P_\theta \psi(t,r,\theta) = 0$.

The equations for f, ψ and the perturbation of the conduction state temperature, $\Theta = T - T_\mathrm{c}$, are

$$\begin{pmatrix} I & 0 & 0 \\ 0 & I & 0 \\ 0 & 0 & \Delta \end{pmatrix} \partial_t \begin{pmatrix} f \\ \Theta \\ \psi \end{pmatrix} = \begin{pmatrix} \sigma\tilde{\Delta} & 0 & 0 \\ 0 & \Delta & -(r^2 \ln\eta)^{-1}\partial_\theta \\ 0 & \sigma r^{-1} Ra \partial_\theta & \sigma\Delta\Delta \end{pmatrix} \begin{pmatrix} f \\ \Theta \\ \psi \end{pmatrix} + \begin{pmatrix} P_\theta[\Delta\psi\partial_\theta\psi]/r \\ J(\psi,\Theta) - f\partial_\theta\Theta/r \\ (1-P_\theta)J(\psi,\Delta\psi) + \tilde{\Delta} f\partial_\theta\psi/r - f\partial_\theta\Delta\psi/r \end{pmatrix}, \tag{19}$$

where $\Delta = (\partial_r + 1/r)\partial_r + (1/r^2)\partial^2_{\theta\theta}$, $\tilde{\Delta} = \partial_r(\partial_r + 1/r)$, and $J(h,g) = (\partial_r h \partial_\theta g - \partial_r g \partial_\theta h)/r$. With this formulation, the no-slip boundary conditions for the velocity become $f = \psi = \partial_r\psi = 0$, and the temperature perturbation is $\Theta = 0$, on both boundaries. See [26] for details.

A simple inspection reveals that the system is O(2)-equivariant under arbitrary rotations of angle θ_0,

$$R_{\theta_0} : (f, \Theta, \psi)(r,\theta) \to (f, \Theta, \psi)(r, \theta + \theta_0) \tag{20}$$

and reflections with respect to diameters $\theta = \theta_0$,

$$\zeta_{\theta_0} : (f, \Theta, \psi)(r,\theta) \to (-f, \Theta, -\psi)(r, 2\theta_0 - \theta). \tag{21}$$

These symmetries are responsible for the large number of bifurcations found in the problem.

We use spectral methods [4] to discretize (19); ψ and Θ are approximated by Fourier expansions in θ

$$\psi = \psi(t,r,\theta) = \mathrm{i}\sum_{\substack{n=-N/2 \\ n\neq 0}}^{N/2} \psi_n(t,r)\mathrm{e}^{\mathrm{i}n\theta},$$

$$\Theta = \Theta(t,r,\theta) = \sum_{n=-N/2}^{N/2} \Theta_n(t,r)\mathrm{e}^{\mathrm{i}n\theta},$$

$\psi_n(t,r)$ and $\Theta_n(t,r)$ being polynomials of degree L in r that verify the boundary conditions. The unknowns of the problem are the values of $f(t,r), \psi_n(t,r)$ and $\Theta_n(t,r)$ on the mesh of Gauss–Lobatto points $r_j = r_\mathrm{i} + (1-\cos(\pi j/L))/2$, with $j = 1,\ldots,L-1$ for f and Θ_n, and $j = 2,\ldots,L-2$ for ψ_n. The total number is then $(L-1)(N+2)+(L-3)N$.

The truncation parameters L and N have been chosen to minimize the computational cost, but keeping the relevant features of the problem well resolved. In the results shown, $L\times N = 32\times 192$ for a total of 11,582 unknowns. By using only the time integration code and comparing with resolutions 32×256 and 48×192, we have found differences below 0.2% for the worst resolved frequency of the quasi-periodic solutions obtained above $Ra = 18,000$ (see Table 1 in [27]). With the same truncations, we have also estimated differences below 0.5% in the Rayleigh numbers of the bifurcation points between stable solutions up to $Ra = 21,000$ used as a test. In addition, for a periodic orbit at $Ra = 17,194$ computed by parameter continuation with truncations 32×192 and 64×256, the frequency difference is below 0.1%. For this solution, Fig. 1 shows the exponential decay of the coefficients of Θ and ψ when Θ_n and ψ_n are expanded in Chebyshev polynomials, i.e., $\Theta_n(t,r) = \sum_{l=0}^{L}\Theta_{l,n}(t)T_l(x)$ with $x = 2(r-r_\mathrm{i})-1$. The maximum resolution employed has been 64×256, giving a total of 31,870 unknowns. The algorithms still work properly, but the CPU time needed to integrate the equations increases considerably due to the need of reducing the time step in order to keep the stability of the numerical integration scheme employed, and due to the increase in the cost of the evaluation of the nonlinear terms and of the solution of the linear systems in (24).

The nonlinear terms of the equations are evaluated by using trigonometric interpolation and FFT techniques for the azimuthal operators, and matrix–matrix products to evaluate radial operators. These

Table 1
Integration coefficients of the BDF-extrapolation formulae

Coefficients	Order					
	1st ($\gamma_0 = 1$)	2nd ($\gamma_0 = 3/2$)	3rd ($\gamma_0 = 11/6$)	4th ($\gamma_0 = 25/12$)	5th ($\gamma_0 = 137/60$)	6th ($\gamma_0 = 147/60$)
α_0	1	2	3	4	5	6
α_1	0	−1/2	−3/2	−3	−5	−15/2
α_2	0	0	1/3	4/3	10/3	20/3
α_3	0	0	0	−1/4	−5/4	−15/4
α_4	0	0	0	0	1/5	6/5
α_5	0	0	0	0	0	−1/6
β_0	1	2	3	4	5	6
β_1	0	−1	−3	−6	−10	−15
β_2	0	0	1	4	10	20
β_3	0	0	0	−1	−5	−15
β_4	0	0	0	0	1	6
β_5	0	0	0	0	0	−1

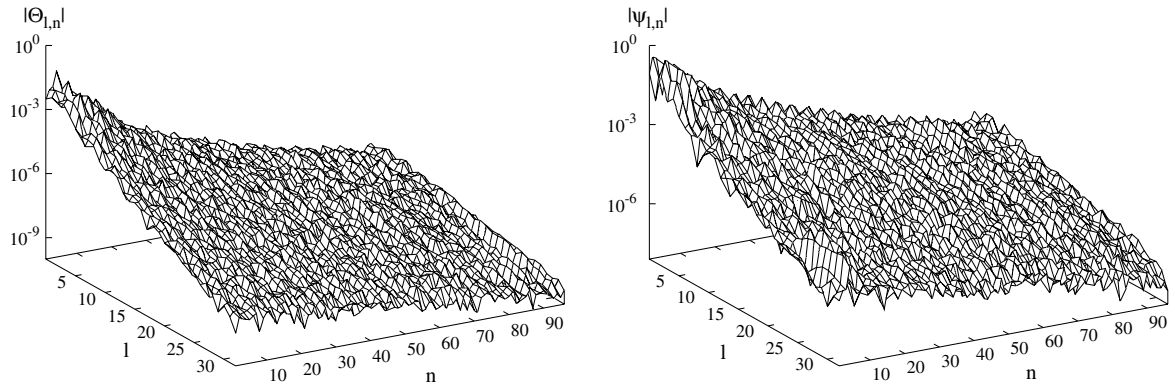

Fig. 1. Decay of the expansion in Chebyshev and Fourier coefficients of a periodic solution at $Ra = 17,194$. See its location in the bifurcation diagram of Fig. 4.

products are performed by the ATLAS [42] version of the DGEMM routine of the BLAS library [18], optimized for Pentium processors (all computations have been performed on Pentium IV PC's at 1.8 GHz). For time integration, backward differentiation formulae (BDF) for the linear part of (19) and extrapolation formulae for the nonlinear terms are used [13]. The BDF-extrapolation formulae, with a fixed time step, Δt, for the system

$$\mathscr{B}\dot{u} = \mathscr{L}u + \mathscr{N}(u), \tag{22}$$

where $\mathscr{L}$ and $\mathscr{N}$ are linear and nonlinear operators respectively, are

$$\frac{1}{\Delta t}\mathscr{B}\left(\gamma_0 u^{n+1} - \sum_{i=0}^{k-1}\alpha_i u^{n-i}\right) = \sum_{i=0}^{k-1}\beta_i \mathscr{N}(u^{n-i}) + \mathscr{L}u^{n+1}, \tag{23}$$

or rearranging,

$$\left(\frac{\gamma_0}{\Delta t}\mathscr{B} - \mathscr{L}\right)u^{n+1} = \mathscr{B}\left(\frac{1}{\Delta t}\sum_{i=0}^{k-1}\alpha_i u^{n-i}\right) + \sum_{i=0}^{k-1}\beta_i \mathscr{N}(u^{n-i}). \tag{24}$$

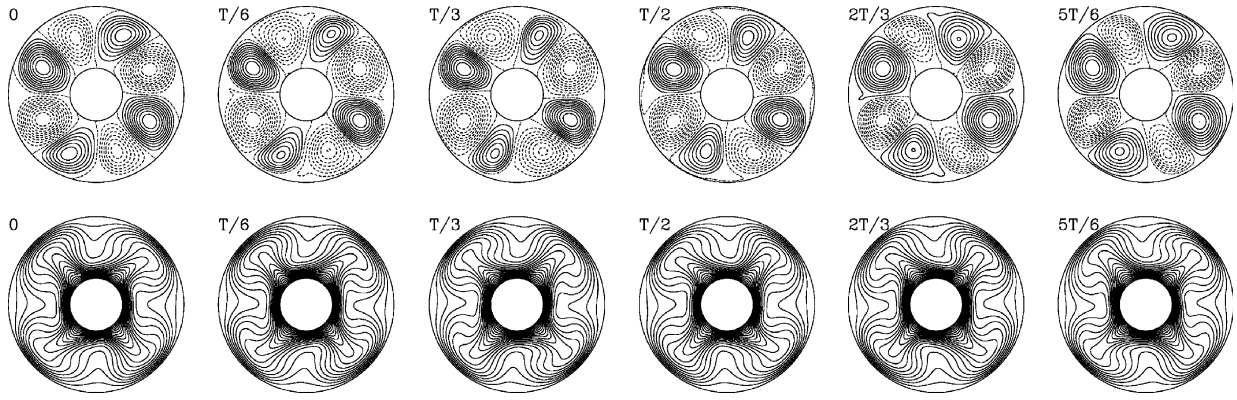

Fig. 2. Time evolution of a symmetric cycle at $Ra = 17,761$ showing the spatio-temporal symmetries of the solution. Upper row: Contour plots of the stream function. Lower row: Contour plots of the temperature. See the location of the solution in the bifurcation diagram of Fig. 4.

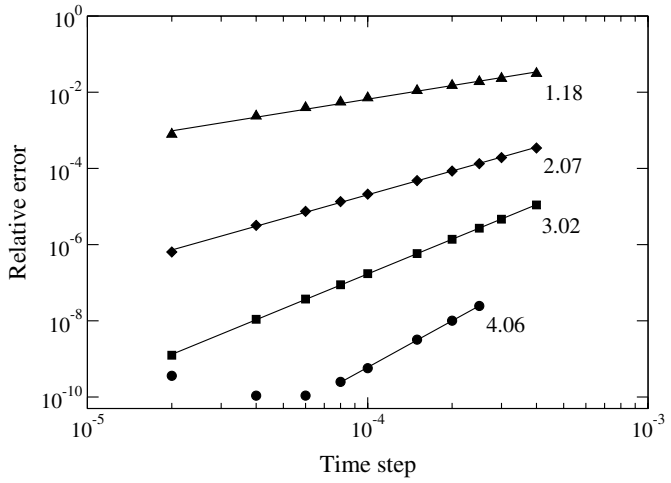

Fig. 3. Test of the order of the time integration method for $Ra = 8000$.

The coefficients α_i, β_i and γ_0 are listed in Table 1. We have always used the fourth order formula in the computations shown. Each time step involves one evaluation of the nonlinear terms, one of the left hand side operator $\mathscr{B}$, and the solution of a linear system with matrix $(\gamma_0/\Delta t)\mathscr{B} - \mathscr{L}$, which, in our case, is block diagonal.

Two different methods have been employed to find the starting values $u^1, \ldots, u^{k+1}$ needed to apply (24); a fourth order Runge–Kutta scheme with a smaller time step, or a procedure involving increasing time steps and orders. We have not found significant differences in precision or CPU time between the two methods.

Fig. 3 shows a numerical study of the precision that can be obtained with this integration scheme for the test problem. It shows the dependence of the relative difference,

$$\frac{||u_{\Delta t} - u_{\mathrm{ref}}||_2}{||u_{\mathrm{ref}}||_2},$$

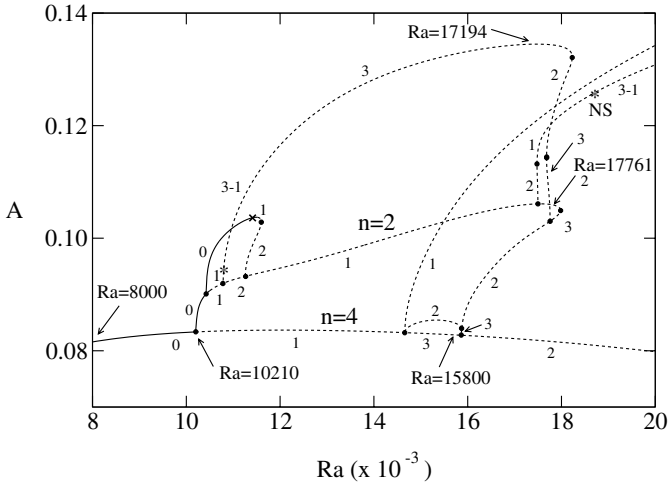

Fig. 4. Diagram of bifurcations of periodic orbits for the annulus problem. See the text for the meaning of the amplitude A. The solid circles correspond to turning points and branching points of periodic orbits, the cross to a bifurcation very close to a non-generic double +1 bifurcation and the asterisks to Neimark–Sacker bifurcations. The arrows indicate the location of the solutions plotted in Figs. 2, 6 and 7, and of the solution for which the test of Fig. 3 has been made.

on Δt. We denote as $u_{\Delta t}$ the solution calculated with time step Δt, and u_{ref} is a reference solution obtained with $\Delta t = 10^{-5}$. The initial condition for both is taken on a periodic solution of the system with $Ra = 8000$ (see its location in the bifurcation diagram of Fig. 4), and the total time integration is twice the period of the orbit. Each curve corresponds to the integration with a different order of the BDF-extrapolation formulae, and the order obtained is used to label them. The results shown have been obtained by initializing the integration with a fourth order Runge–Kutta method. It can be seen that below $\Delta t = 8 \times 10^{-5}$ the propagation of the rounding errors, generated mainly in the evaluation of the nonlinear terms and in the initialization process, do not allow us to obtain relative errors below 10^{-10}. It must be pointed out that the matrix of the derivatives in the radial direction, and some formulae employed to apply the boundary conditions, are prone to cancellation errors, and that the code employs the 3/2-rule dealiasing technique in the azimuthal coordinate.

In this particular problem, the solutions of $x = P(x)$ are determined up to an azimuthal rotation. Therefore a phase condition must be added to obtain a determinate system of equations. For this purpose one of the equations is replaced by a condition that selects the solution closest to a previous reference solution x_{ref}. It is easy to see that this condition can be written as the linear equation $x_{\text{ref}}^{\mathrm{T}} \partial_\theta x = 0$. It is similar to the phase condition used in some continuation codes for periodic orbits to fix the initial point on the orbit [15].

The periodic orbits we have found in this problem are known as direction reversing travelling waves [17] (DRTW), or as symmetric cycles (S-cycles) in the dynamical systems context, i.e., they have the following spatio-temporal symmetry

$$\begin{aligned} \Theta(t,r,\theta) &= \Theta(t+T/2,r,2\theta_0-\theta), \\ f(t,r) &= -f(t+T/2,r), \\ \psi(t,r,\theta) &= -\psi(t+T/2,r,2\theta_0-\theta), \end{aligned} \tag{25}$$

where T is the period of the orbit, and θ_0 is fixed by the initial conditions. For these periodic orbits the evolution by half a period in time is equivalent to the reflection defined in (21) with respect to a certain diameter. This can be seen in Fig. 2. It shows the time evolution of a S-cycle obtained at $Ra = 17,761$, for which $\theta_0 \approx \pi/2$. See also [27] for shadowgraph space-time plots.

As f changes sign each half period (25), the net mass flow defined as

$$\frac{1}{R_{\text{o}} - R_{\text{i}}} \int_{R_{\text{i}}}^{R_{\text{o}}} \mathbf{u}_\theta(t,r,\theta)\mathrm{d}r = \frac{1}{R_{\text{o}} - R_{\text{i}}} \int_{R_{\text{i}}}^{R_{\text{o}}} f(t,r)\mathrm{d}r \tag{26}$$

changes sign twice per period. Therefore, the approximation to the zero net mass flow condition, $\sum_{j=0}^{L} w_j f(t,r_j) = 0$, where the w_j are the weights of the Gauss–Lobatto quadrature formulae, has been used to define the hyperplane Σ on which the Poincaré map is taken. Consequently, there has been no need to change the hyperplane during the continuation, as might be required when periodic orbits without symmetries are sought.

4. Results

Before presenting the results we want to stress that the main goal of this paper is the presentation of a method to efficiently compute periodic orbits for Navier–Stokes flows. The reader interested in a more complete bifurcation diagram, in the attractors for the range of Ra studied or in the coexistence of attractors for a fixed Ra, can find this information in [27]. Still many details are missing, mainly concerning the continuation of unstable tori.

Fig. 4 shows the branches of the periodic orbits we have found in the test problem. A weighted amplitude

$$A = \sum_{n=0}^{4} w_n |\Theta_n(r_p)|$$

of the first five azimuthal modes of the temperature perturbation, at the time at which the net mass flow vanishes on Σ, versus the Rayleigh number has been plotted. In A, r_p is a fixed radial point, and the weights, w_n, are selected to clearly distinguish the different branches. Solutions related by the spatial symmetries broken at the bifurcations correspond to the same points in the diagram. Beside each branch we indicate the number of multipliers outside the unit circle. If all of them are real we use a single number. When there are complex pairs we indicate the total number of unstable multipliers by the first number followed by the number of those real.

The main branch is labeled $n = 4$ because only the azimuthal Fourier coefficients of ψ and Θ with subscripts n which are multiple of 4 are non-zero. It bifurcates from a stable steady solution through a Hopf bifurcation, after the spatial interaction of steady $n = 2$ and $n = 4$ modes described in [27]. The isotropy group of these steady solutions (the group of transformations that leave them invariant) is generated by a reflection by a diameter and a rotation of $\pi/2$. Fig. 5 shows one of them at $Ra = 6300$. In this and all the following figures, the leftmost plot corresponds to the contour plot of ψ, the centre one to the isotherms, and the rightmost to the lines of constant Θ. For the periodic solutions (Figs. 6, 7 and 9), the plots show the data when they cross the Poincaré section.

The periodic orbits are no longer reflection symmetric (see Fig. 6 as example), and consequently [17] are DRTWs that oscillate back and forth in the azimuthal direction without net drift. For this type of solution, the spatio-temporal symmetry (25) could have been used to halve the time needed to compute each orbit, but we have always integrated the whole period, because we are describing a general methodology, and we did not know in advance that all the bifurcations between branches of periodic orbits were going to break only spatial symmetries in the range of Ra considered. Information about the origin and the physical behavior of these solutions can be found in [27].

All the periodic solutions of the test problem have a $\mu = +1$ multiplier due to the invariance under rotations of the equations. It has been removed in all the plots of the spectra shown, and because it never crosses the unit circle, it is not considered in the following count of the critical multipliers. It is known [15] that S-cycles cannot experience period doubling bifurcations through simple $\mu_1 = -1$ multipliers. In agreement with this result, only bifurcations with $\mu_1 = +1$ or $\mu_{1,2} = e^{\pm i\theta_0}$ were found. The turning points and the branching points of periodic orbits have been marked with full circles; the other intersections are due to the graphical representation. The D_4 symmetry forces the second point on the $n = 4$ branch to be double, and two other points are very close to non-generic real double +1 bifurcations. This is so in the bifurcation marked with a cross on the smallest loop of Fig. 4, and in the second bifurcation point on the $n = 2$ branch. In both cases, two complex-conjugate multipliers of diminishing frequency become real very

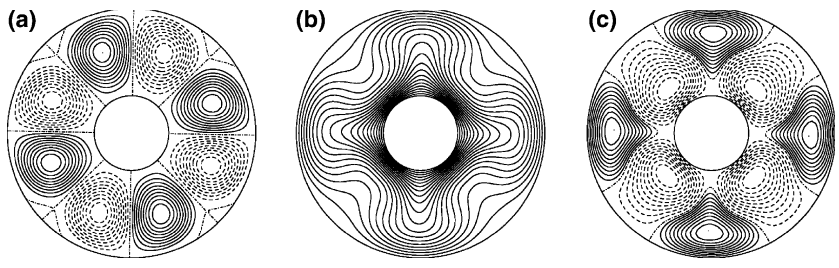

Fig. 5. Contour plots of the streamfunction, the temperature and the temperature perturbation for a steady solution at $Ra = 6300$.

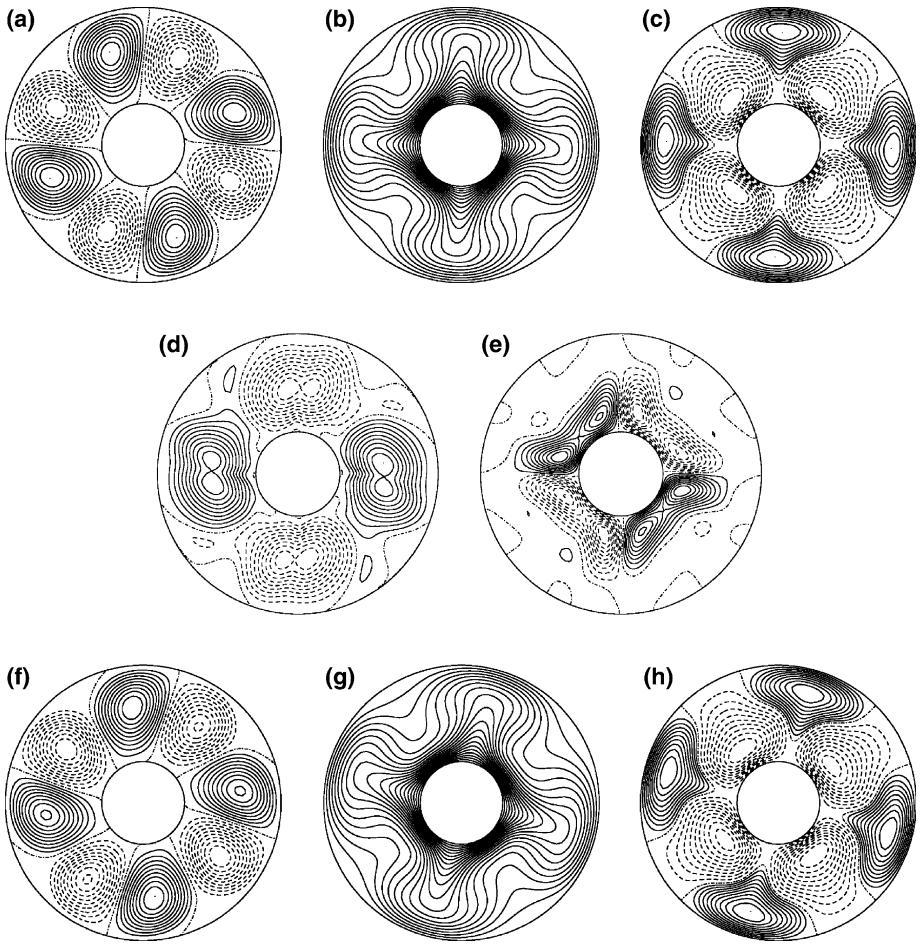

Fig. 6. Contour plots of the streamfunction, the temperature and the temperature perturbation; (a, b, c) for the stable pure $n = 4$ branch of DRTW at $Ra = 10,200$, and (f, g, h) for the stable subharmonic DRTW at $Ra = 10,225$. (d, e) Dominant eigenfunction of the first multiplier that crosses the unit circle at $Ra = 10,210$. (d) corresponds to the contour plot of the streamfunction and (e) to that of the temperature perturbation.

near the unit circle ($\mu_{1,2} = 0.996$ and $\mu_{1,2} = 0.994$, respectively). By increasing Ra, one of them grows and crosses the unit circle while the other moves back. By slightly moving another parameter of the problem, for instance the radius ratio, the complex multipliers would become real exactly on the unit circle. The difference between the two transitions is the symmetry group of the periodic orbits that bifurcate. In the diagram, there are, moreover, two Neimark–Sacker bifurcations in the interval of Ra considered. They are indicated with asterisks at $Ra = 10,785$ and $Ra = 18,683$.

The detailed description of all the bifurcations is beyond the scope of this paper; nevertheless we have selected some of them to show the accuracy obtained in the solutions and in their spectra. As an example of the spatial structure of the solutions, we display in Fig. 6 the first symmetry breaking bifurcation, and in Fig. 7 some samples of solutions on the most unstable branches at higher parameter values.

The pure $n = 4$ DRTWs that appear at $Ra = 6897$ maintain a $R_{\pi/2}$-invariance;

$$\Theta(t, r, \theta) = \Theta(t, r, \theta + \pi/2), \quad \psi(t, r, \theta) = \psi(t, r, \theta + \pi/2),$$

but they are no longer reflection symmetric as can be seen in the plots of Fig. 6(a)–(c). The $n = 4$ DRTW is stable up to $Ra = 10,210$, where it loses stability in a subharmonic pitchfork bifurcation of periodic orbits.

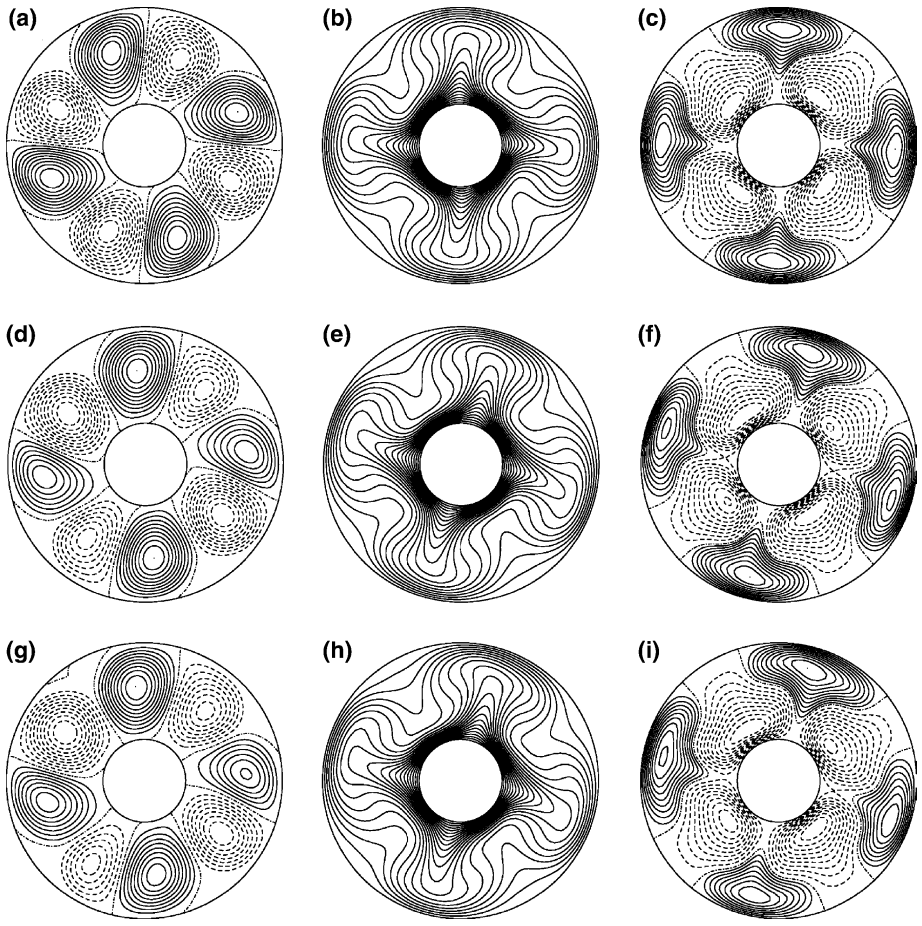

Fig. 7. Contour plots of the streamfunction, the temperature and the temperature perturbation; (a, b, c) for a solution on the $n = 4$ branch at $Ra = 15,800$; (d, e, f) for a solution on the $n = 2$ branch at $Ra = 17,761$, and (g, h, i) for a solution with no spatial symmetries at $Ra = 17,194$. Their locations are marked with an arrow in Fig. 4.

This is a symmetry breaking bifurcation that reduces the spatial $\mathbb{Z}_4$ isotropy group to $\mathbb{Z}_2$, where $\mathbb{Z}_4$ and $\mathbb{Z}_2$ are generated by rotations of $\pi/2$ and π, respectively. The symmetric branches of the pitchfork bifurcation are related by a rotation of $\pi/2$. The change of symmetry can be observed in the dominant eigenfunction of Fig. 6(d) and (e), and in the stable subharmonic $n = 2$ DRTW of Fig. 6(f)–(h), if it is carefully observed. In the plots of the eigenfunction the isotherms are omitted.

Fig. 7 shows a sample of the most unstable solutions found with $\sigma = 0.025$ and $\eta = 0.3$. All of them have three unstable multipliers and they are on three different branches. Their locations at $Ra = 15,800$, 17,761 and 17,194 are indicated with arrows in Fig. 4. Their isotropy groups of spatial symmetries are $\mathbb{Z}_4$, $\mathbb{Z}_2$ and trivial, respectively, as can be seen better in the contour plots of the streamfunction. In addition, their leading multipliers are displayed in Fig. 8, where the dotted line is the unit circle. In Fig. 8(a) the leading multiplier is double.

The spectrum of the Neimark–Sacker bifurcation, indicated in Fig. 4 with an asterisk at $Ra = 18,683$, is in agreement with the results computed with the time evolution code. By decreasing Ra with this code, we have found a saddle-node bifurcation of tori at $Ra \approx 18,440$. We believe that this stable branch of tori is connected with the periodic orbits we have computed through the Neimark–Sacker bifurcation, because of the agreement between the frequency determined from the dominant unstable multiplier and the second frequency of the quasi-periodic solutions calculated. The results indicate that at the bifurcation point, a

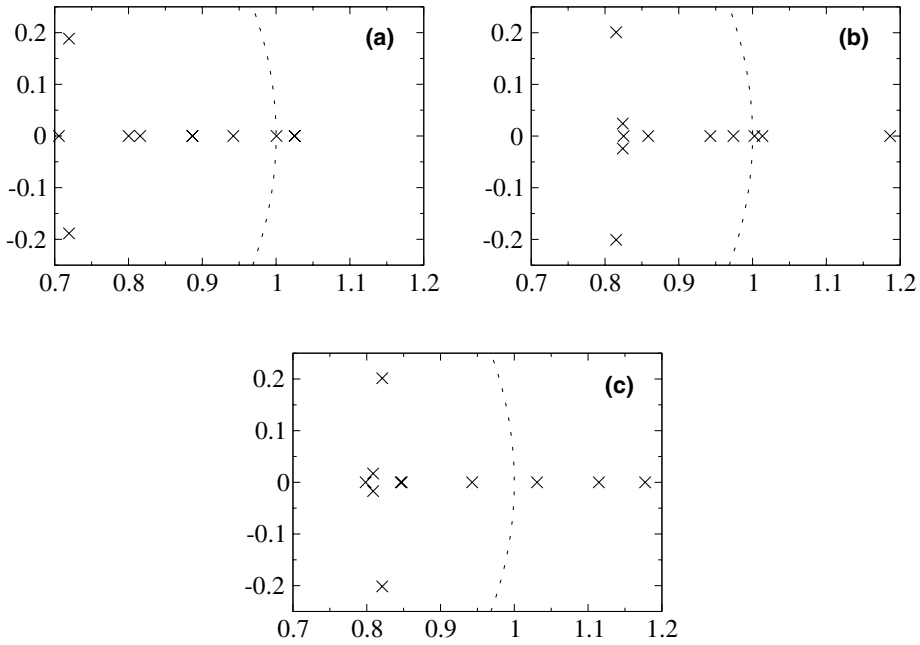

Fig. 8. Leading Floquet multipliers of the solutions represented in Fig. 7; (a) $Ra = 15,800$ (the leading multiplier is double), (b) $Ra = 17,761$, and (c) $Ra = 17,194$.

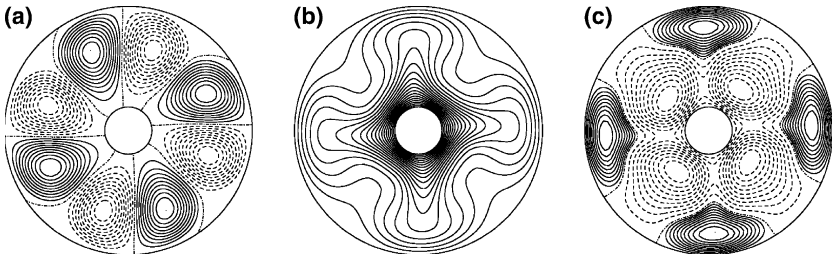

Fig. 9. Contour plots of (a) the streamfunction, (b) the temperature and (c) the temperature perturbation for the DRTW at $Ra = 20,000$ and $\eta = 0.19$.

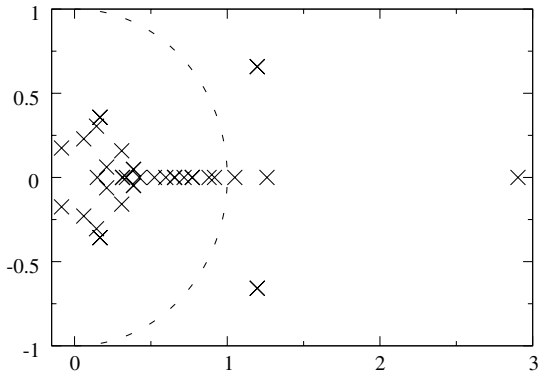

Fig. 10. Leading Floquet multipliers of the solution represented in Fig. 9. The complex pair outside the unit circle is double.

branch of unstable quasi-periodic solutions appears. This branch becomes stable through a bifurcation (or bifurcations) we have not studied because our present codes do not allow to compute invariant unstable tori. This is an example of an attractor connected through unstable manifolds to other attractors. The main $n = 4$ branch of periodic orbits, which is stable up to $Ra = 10,210$ bifurcates also from a steady solution connected to the trivial conductive solution by unstable fixed points [27].

Calculations with different values of the radius ratio η have also been performed to check if the method still works efficiently for more unstable orbits. We show in Fig. 9 a solution for $\eta = 0.19$ and $Ra = 20,000$. As can be seen in Fig. 10 it has seven unstable multipliers, including a double complex conjugate pair. We have not found any significant change in the computational cost to obtain these more unstable solutions.

5. Efficiency

Table 2 displays the number of iterations of Newton's and GMRES methods needed to refine a periodic solution at $Ra = 17,194$ (see Fig. 4 to locate it in the bifurcation diagram and Fig. 8 to see its leading multipliers). The initial condition had components $x_i(1 + \varepsilon u_i)$, x being a previous refined solution and u a random vector satisfying $|u_i| < 1$, and the value of the parameter λ was kept fixed. Stopping criterion for Newton's method was $||x^{(n+1)} - x^{(n)}||_2/||x^{(n+1)}||_2 < 10^{-8}$ and $||x^{n+1} - P(x^{n+1})||_2 < 10^{-8}$. The dimension of the Krylov subspace was 60, but could have been 51 with the same results, or 34 for $\varepsilon \leqslant 10^{-5}$ without need of restarting. The number of iterations needed by GMRES decrease as Newton's method approaches the solution. This is a common feature with Newton–Krylov methods, when GMRES is started with a zero initial guess.

Good initial conditions for Newton's method must always be provided to have efficient continuations, but in the case of continuation of periodic orbits this is especially important. We recall that the most expensive calculation during the continuation is the evaluation of $\mathrm{DP}(x, \lambda)v$ at each GMRES iteration. Therefore, the predictor should use high-order extrapolation from previous solutions or small parameter or pseudo-arclength steps. The highest suitable extrapolation order depends not only on estimates on the extrapolation error, but also on bounds on the errors in the previous solutions used in the extrapolation. Finding the optimum between computing many solutions at low cost or fewer solutions at higher computational effort is not an easy task, especially if this must be done automatically. The total number of GMRES iterations used to find a solution, not only the number of Newton's iterations, should be used to control the arclength step.

Fig. 11(b)–(e) show the total number of GMRES iterations needed to compute each solution along the portion of branches displayed in Fig. 11(a) (compare this plot with Fig. 4). B_1 is an $n = 4$ branch, i.e., only a quarter of the unknowns are non-zero. A system of dimension 2942 could have been solved, although we did not made use of this particular characteristic. Along B_2 and B_3, all the unknowns are non-zero. B_2 is a regular arc without bifurcations and there are two turning points on B_3, which ends at a bifurcation point. With this selection we explore all possible scenarios in the bifurcation diagram.

Table 2
Number of Newton's and GMRES iterations when computing the solution of Fig. 7 (g)–(i) at $Ra = 17,194$

ε	Newton iterations	GMRES iterations	CPU time (s)
10^{-4}	6	51, 48, 49, 47, 27, 1	12,004
10^{-5}	3	34, 12, 1	2779
10^{-6}	2	30, 1	1845
10^{-7}	2	17, 1	1184
10^{-8}	2	9, 1	780

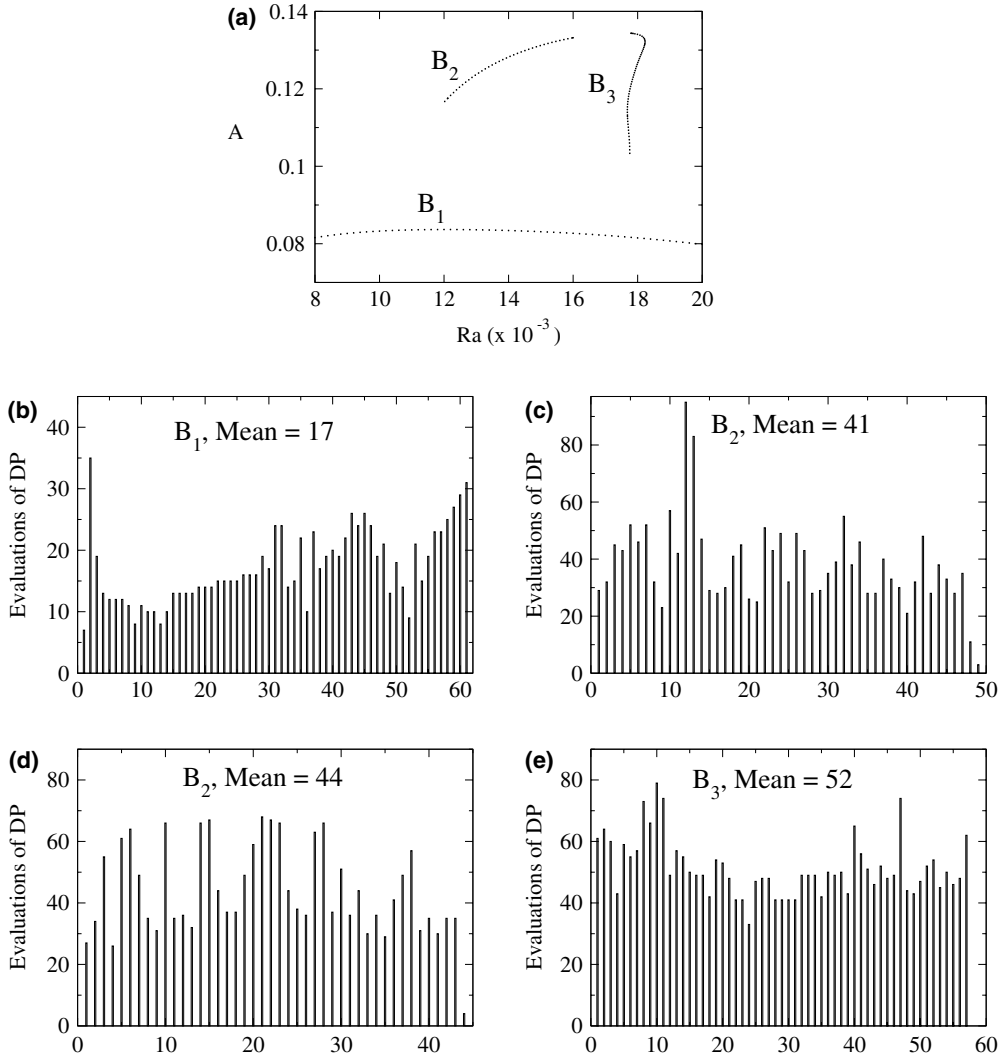

Fig. 11. (a) Branches of periodic orbits used to study the efficiency of the method (see also Fig. 4). Number of evaluations of $DP(x)v$ needed to compute each point along branches, (b) B_1 with parameter continuation, (c) B_2 with parameter continuation, (d) B_2 but with pseudo-arclength continuation, and (e) B_3 with pseudo-arclength continuation.

In all these calculations, the time step used was 10^{-4}, and the stopping criterion for Newton's method was

$$||(x,\lambda)^{(n+1)} - (x,\lambda)^{(n)}||_w / ||(x,\lambda)^{(n+1)}||_w < 10^{-7}, \quad \text{and} \tag{27}$$

$$||(x^{(n+1)} - P(x^{n+1},\lambda^{(n+1)}), n(x^{(n+1)},\lambda^{(n+1)}))||_w < 10^{-7} \tag{28}$$

with $||(z,\mu)||_w = (||z||_2^2 + (w|\mu|)^2)^{1/2}$ a weighted norm.

Four cases have been considered. Fig. 11(b) corresponds to branch B_1 calculated by using parameter continuation and a fixed parameter step size of 200. For this branch the mean of the total number of GMRES iterations is 17. Branch B_2 was calculated with both parameter (Fig. 11(c)) and pseudo-arclength (Fig. 11(d)) continuation. The average number of evaluations of $DP(x,\lambda)v$ was very similar for both cases; 41 and 44, respectively. B_3 was only computed by pseudo-arclength continuation (Fig. 11(e)) due to the

presence of the turning points. The mean number of GMRES iterations increased up to 52. This branch is more expensive to compute because the solutions change significantly through the turning points and there are multipliers near +1 along all the curve.

The CPU times to complete each of these calculations were 22.2, 37.5, 38.8 and 100 h, respectively. Each evaluation of $DP(x,\lambda)v$ took between 50 and 170 s depending on the branch considered. Then the CPU time to compute each periodic orbit in the diagram of Fig. 4 varied from 10 to 90 min.

To obtain the 40 leading Floquet multipliers shown in Fig. 10, 100 evaluations of $DP(x,\lambda)v$ were required when using the ARPACK library. This is more than has been usually required to obtain the information needed to study the bifurcations and complete the diagram of Fig. 4. Only the calculation of the first 12 multipliers was used to detect the bifurcations, and each spectra needed between 40 and 80 matrix–vector products (i.e., time integrations of system (12)) depending strongly on the separation between the required eigenvalues and the rest of them, and on the dimension of the Krylov subspace.

6. Conclusions and perspectives

We have shown that the Newton–Krylov method, applied to find fixed points of Poincaré maps of high-dimensional dissipative systems, provides an efficient, easy to implement, and robust tool to compute periodic orbits. A complicated bifurcation diagram of periodic orbits, most of them unstable, for a system of dimension 11,582 has been obtained. Comparison with the Newton–Picard method is not easy because, in the method we use, finding the cycles and studying their stability are separate processes. The Newton–Picard method requires the computation of a good basis of the invariant subspace corresponding to the leading eigenvalues. This is an expensive task even using the most sophisticated versions of subspace iteration or Arnoldi methods, but the stability of the solution is also obtained. By using the Newton–Krylov method we retain the quadratic convergence of the Newton's iterations except, of course, near bifurcation points. This is important to minimize the number of evaluations of the differential of the Poincaré map where almost all the computing time is spent. But surely, the main advantage of using the Newton–Krylov method is its simplicity when compared with other options.

The procedure described in this paper might also be used to find steady solutions of (1). The technique which is usually employed is to apply Newton's method

$$x^{i+1} = x^i + \Delta x^i, \tag{29}$$

$$D_x f(x^i,\lambda)\Delta x^i = -f(x^i,\lambda), \tag{30}$$

to the equation $f(x,\lambda) = L(\lambda)x + Q(x,x) + F = 0$, and to apply a matrix-free iterative method to solve the linear system, preconditioned with $L(\lambda)^{-1}$ or approximations to this operator (see [3,5,23]), i.e.,

$$(I + L(\lambda)^{-1}(Q(x^i,\cdot) + Q(\cdot,x^i)))\Delta x^i = -L(\lambda)^{-1} f(x^i,\lambda) \tag{31}$$

This procedure can be satisfactory near $x = 0$, where the matrix

$$I + L(\lambda)^{-1}(Q(x^i,\cdot) + Q(\cdot,x^i))$$

is a small perturbation of the identity. Far away from $x = 0$, the iterative method to solve (30) might fail to converge. As stated in the introduction, if finite differences or finite elements are employed, an incomplete LU decomposition can be used as preconditioner to accelerate the convergence. In the case of spectral methods it is not easy to find good preconditioners. Finite differences or finite elements versions of the problem have been successfully used as preconditioners but the coding becomes more complicated. We

suggest a simple, although in general more expensive approach, that can be used when other possibilities fail.

Let $\varphi(t,x,\lambda)$ be the solution of (1) with initial condition x, T a positive real number, and define now $P(x,\lambda) = \varphi(T,x,\lambda)$. If x_0 is a fixed point of $f, f(x_0,\lambda_0) = 0$ then $x_0 - P(x_0,\lambda_0) = 0$. The equation $x - P(x,\lambda) = 0$ can be solved by the Newton–Krylov method. Now, as in the case of periodic orbits, if the initial system is dissipative, the spectrum of the matrix $I - D_x P(x,\lambda)$ is clustered around $z = 1$. The products $D_x P(x,\lambda)v$ are calculated by using (14), but replacing $t(x)$ by T. T is a parameter which must be selected to make convergence fast. It should not be large if the fixed point x_0 is very unstable. If it is stable, the method can be seen as an acceleration of the time evolution toward the steady state. If x_0 is unstable, it is an stabilization method very close in spirit to the condensation method of Jarausch and Mackens [11], or the RPM of Shroff and Keller [33]. It has been used to complete some of the branches of steady solutions in the annular problem [27]. Other invariant manifolds could also be computed by using the same ideas here described. In particular we are interested in extending the techniques employed in [35] and [12] to compute invariant tori for, at least, moderate-dimensional problems.

It is known that simple shooting might not work for very unstable periodic orbits [37]; then multiple shooting should be used. Its implementation, with the method described in this work, is quite straightforward. Even if the solutions are not very unstable, multiple shooting could be used with each shoot computed in parallel on a different processor. Almost all the CPU time is spent in time integrations; therefore, this seems the only way of using parallelism efficiently, on computers with relatively slow communications between processors as in Beowulf clusters. None of the periodic orbits calculated in this paper has required the use of multiple shooting.

We have only used GMRES to solve the linear systems but other possibilities, BICGSTAB(l) [36] for instance, could be considered. They could improve the convergence and reduce the storage requirements. For branches of periodic orbits along which there are always multipliers very close to +1, the convergence of the iterative linear solvers could be improved by using information on the leading eigenpairs to build a preconditioner. Some of these issues are now being studied.

Acknowledgements

The research of J.S. and M.N. has been supported by DGICYT project BFM2001-2336. The research of B.G.-A. has been supported by DGICYT projects PB98-0072 and BFM2003-00336. The research of C.S. has been supported by DGICYT projects BFM2000-805 and BFM2003-09504-C02-01 and grant CIRIT 2001SGR-70.

References

[1] D. Barkley, R.D. Henderson, Floquet stability analysis of the periodic wake of a circular cylinder, J. Fluid Mech. 322 (1996) 215–241.
[2] K. Böhmer, Z. Mei, A. Schwarzer, R. Sebastian, Path-following of large bifurcation problems with iterative methods, in: E. Doedel, L.S. Tuckerman (Eds.), Numerical methods for bifurcation problems and large-scale dynamical systems, volume 119 of The IMA volumes in Mathematics and its Applications, Springer, Berlin, 2000, pp. 35–65.
[3] P.N. Brown, Y. Saad, Hybrid Krylov methods for nonlinear systems of equations, SIAM J. Sci. Stat. Comput. 11 (3) (1990) 450–481.
[4] C. Canuto, M.Y. Hussaini, A. Quarteroni, T.A. Zang, Spectral Methods in Fluid Dynamics, Springer, Berlin, 1988.
[5] G.F. Carey, K. Wang, W. Joubert, Performance of iterative methods for Newtonian and generalized Newtonian flows, Int. J. Numer. Meth. Fluids 9 (1989) 127–150.
[6] R.S. Dembo, S.C. Eisenstat, T. Steihaug, Inexact Newton methods, SIAM J. Numer. Anal. 19 (2) (1982) 400–408.

[7] E. Doedel, AUTO: Software for continuation and bifurcation problems in ordinary differential equations. Report Applied Mathematics, California Institute of Technology, Pasadena, USA, 1986.
[8] W.S. Edwards, L.S. Tuckerman, R.A. Friesner, D.C. Sorensen, Krylov methods for the incompressible Navier–Stokes equations, J. Comput. Phys. 110 (1994) 82–102.
[9] J. Guckenheimer, M.R. Myers, F.J. Wicklin, P.A. WorfSolk, DsTool: A dynamical system toolkit with an interactive graphical interface. Center for Applied Mathematics, Cornell University, Ithaca, NY, USA, 1995.
[10] R.D. Henderson, D. Barkley, Secondary instability in the wake of a circular cylinder, Phys. Fluids 8 (1996) 1683–1685.
[11] H. Jarausch, W. Mackens, Solving large nonlinear systems of equations by an adaptive condensation process, Numer. Math. 50 (6) (1987) 633–653.
[12] A. Jorba, Numerical computation of the normal behaviour of invariant curves on n-dimensional maps, Nonlinearity 14 (2001) 943–976.
[13] G.E. Karniadakis, M. Israeli, S.A. Orszag, High-order splitting methods for the incompressible Navier–Stokes equations, J. Comput. Phys. 97 (1991) 414–443.
[14] H.B. Keller, Numerical solution of bifurcation and nonlinear eigenvalue problems, in: P.H. Rabinowitz (Ed.), Applications of Bifurcation Theory, Academic Press, New York, 1977, pp. 359–384.
[15] Y.A. Kuznetsov, Elements of Applied Bifurcation Theory, second ed., Springer, New York, 1998.
[16] Y.A. Kuznetsov, V.V. Levitin, CONTENT, a multiplatform continuation environment, Technical report, CWI, Amsterdam, The Netherlands, 1996.
[17] A.S. Landsberg, E. Knobloch, Direction-reversing travelling waves, Phys. Lett. A 159 (1991) 17–20.
[18] C. Lawson, R. Hanson, D. Kinkaid, F. Krogh, Basic linear algebra subprograms for FORTRAN usage, ACM Trans. Math. Soft. 5 (3) (1979) 308–325.
[19] R.B. Lehoucq, D.C. Sorensen, Deflation techniques for an implicitly restarted Arnoldi iteration, SJMAA 17 (1996) 789–821.
[20] R.B. Lehoucq, D.C. Sorensen, C. Yang, ARPACK User's Guide: Solution of Large-Scale Eigenvalue Problems with Implicitly Restarted Arnoldi Methods, SIAM, 1998.
[21] J.M. Lopez, F. Marqués, J. Sánchez, Oscillatory modes in an enclosed swirling flow, J. Fluid Mech. 439 (2001) 109–129.
[22] K. Lust, D. Roose, A. Spence, A.R. Champneys, An adaptive Newton–Picard algorithm with subspace iteration for computing periodic solutions, SIAM J. Sci. Comput. 19 (4) (1998) 1188–1209.
[23] C.K. Mamun, L.S. Tuckerman, Asymmetry and Hopf bifurcation in spherical Couette flow, Phys. Fluids 7 (1995) 80–91.
[24] K. Meerbergen, D. Roose, Matrix transformations for computing rightmost eigenvalues of large sparse non-symmetric eigenvalue problems, IMA J. Numer. Anal. 16 (3) (1996) 297–346.
[25] M.J. Molemaker, H.A. Dijkstra, Multiple equilibria and stability of the North-Atlantic wind-driven ocean circulation, in: E. Doedel, L.S. Tuckerman (Eds.), Numerical methods for bifurcation problems and large-scale dynamical systems, volume 119 of The IMA Volumes in Mathematics and its Applications, Springer, Berlin, 2000, pp. 35–65.
[26] D. Pino, I. Mercader, M. Net, Thermal and inertial modes of convection in a rapidly rotating annulus, Phys. Rev. E 61 (2) (2000) 1507–1517.
[27] M. Net, A. Alonso, J. Sánchez, From stationary to complex time-dependent flows in two-dimensional annular thermal convection at moderate Rayleigh numbers, Phys. Fluids 15 (5) (2003) 1314–1326.
[28] Y. Saad, Numerical Methods for Large Eigenvalue Problems, Manchester University Press, Manchester, 1992.
[29] Y. Saad, Preconditioned Krylov subspace methods for CFD applications, Technical Report umsi-94-171, Minnesota Supercomputer Institute, Minneapolis, MN 55415, August 1994.
[30] Y. Saad, Iterative Methods for Sparse Linear Systems, PWS pub. company, New York, 1996.
[31] Y. Saad, M.H. Schultz, GMRES: a generalized minimal residual algorithm for solving nonsymmetric linear systems, SIAM J.Sci. Stat. Comput. 7 (1986) 865–869.
[32] J. Sánchez, F. Marqués, J.M. López, A continuation and bifurcation technique for Navier–Stokes flows, J. Comput. Phys. 180 (2002) 78–98.
[33] G.M. Shroff, H.B. Keller, Stabilization of unstable procedures: the recursive projection method, SIAM J. Numer. Anal. 30 (4) (1993) 1099–1120.
[34] C. Simó, Analytical and numerical computation of invariant manifolds, in: C. Benest, C. Froeschlé (Eds.), Modern Methods in Celestial Mechanics, Editions Frontiéres, Dreux, 1990, pp. 285–330, Accessible also at http://www.maia.ub.es/dsg/2004/index.html.
[35] C. Simó, Effective computations in celestial mechanics and astrodynamics, in: V. Rumyantsev, A. Karapetyan (Eds.), Modern Methods of Analytical Mechanics and their Applications, CISM Courses and Lectures 387, Springer, New York, 1998, pp. 55–102.
[36] G.L.G. Sleijpen, D.R. Fokkema, BICGSTAB(L) for linear equations involving unsymmetric matrices with complex spectrum, ETNA 1 (1993) 11–32.
[37] J. Stoer, R. Bulirsch, Introduction to Numerical Analysis, Springer, New York, 1980.

[38] B.A. van de Rotten, S.M. Verduyn Lunel, A limited memory Broyden method to solve high-dimensional systems of nonlinear equations, Technical Report MI 2003-06, Mathematical Institute, University of Leiden, March 2003.
[39] B.A. van de Rotten, S.M. Verduyn Lunel, A. Bliek, Efficient simulation of periodically forced reactors in 2-D, Technical Report MI 2003-13, Mathematical Institute, University of Leiden, August 2003.
[40] T.L. van Noorden, S.M. Verduyn Lunel, A. Bliek, The efficient computation of periodic states of cyclically operated chemical processes, IMA J. Appl. Math. 68 (2003) 149–166.
[41] T.L. van Noorden, S.M. Verduyn Lunel, A. Bliek, A Broyden rank p+1 update continuation method with subspace iteration (accepted for publication), SIAM J. Sci. Comput (2004).
[42] R.C. Whaley, A. Petitet, J. Dongarra, Automated empirical optimization of software and the ATLAS project, Technical Report UT-CS-00-448, Netlib, Lapack working notes, September 2000.